Computer-generated holograms for three-dimensional surface objects with shade and texture

Kyoji Matsushima

Digitally synthetic holograms of surface model objects are investigated for reconstructing three-dimensional objects with shade and texture. The objects in the proposed techniques are composed of planar surfaces, and a property function defined for each surface provides shape and texture. The field emitted from each surface is independently calculated by a method based on rotational transformation of the property function by use of a fast Fourier transform (FFT) and totaled on the hologram. This technique has led to a reduction in computational cost: FFT operation is required only once for calculating a surface. In addition, another technique based on a theoretical model of the brightness of the reconstructed surfaces enables us to shade the surface of a reconstructed object as designed. Optical reconstructions of holograms synthesized by the proposed techniques are demonstrated. © 2005 Optical Society of America

OCIS codes: 090.1760, 090.2870, 090.1970.

1. Introduction

Computer-generated holograms for three-dimensional (3-D) displays, sometimes called digitally synthetic holograms, are desired media for creating 3-D autostereoscopic images of virtual objects. However, the technology suffers from two problems: the necessity for extremely high spatial resolution to fabricate or display the holograms, and long computation times for the creation, especially in full parallax holograms.

For the past decade, techniques using point sources of light have been widely used to calculate object waves.[1,2] This point source method is simple in principle and potentially the most flexible for synthesizing holograms of 3-D objects. However, because it is too time consuming to create full parallax holograms,[3] many methods to reduce the computation time, including geometric symmetry,[4] look-up tables,[3] difference formulas,[5] recurrence formulas,[6] employing computer-graphics hardware,[7] and constructing special CPUs,[8] have been attempted.

Point source methods for calculating spherical waves emitted from point sources are commonly ray oriented. As they trace the ray from a point source to a sampling point on the hologram, the procedure is sometimes referred to as ray tracing.[2] However, there are also wave-oriented methods to calculate object fields in which fields emitted from objects defined as planar segments[9,10] or 3-D distributions of field strength[11] are calculated by methods based on wave optics. The major advantage of wave-oriented methods is that they can use a fast Fourier transform (FFT) for numerical calculations. Therefore the computation time is shorter than for point source methods, especially in full parallax holograms. However, the optical reconstruction of accurately rendered 3-D objects such as a shaded cube, as reported for wave-oriented methods, was not discussed in the papers cited above. This is so because of a lack of well-defined procedures to generate object fields for arbitrarily shaped surfaces that are diffusive and sometimes have texture. The technique for shading the reconstructed object according to such design parameters as the position of the illumination light and the ratio of the surrounding light is also important in creating real 3-D images by wave-oriented methods.

In wave-oriented methods, calculating fields are commonly based on coordinate transformation in Fourier space.[10,11] A similar method based on the Rayleigh–Sommerfeld integral has been reported within the context of free-space beam propagation.[12] Recently, the author reported a more precise formulation and numerical consideration[13] as an extension

The author (matsu@kansai-u.ac.jp) is with the Department of Electrical Engineering and Computer Science, Kansai University, 3-3-35 Yamate-cho, Suita, Osaka 564-8680, Japan.
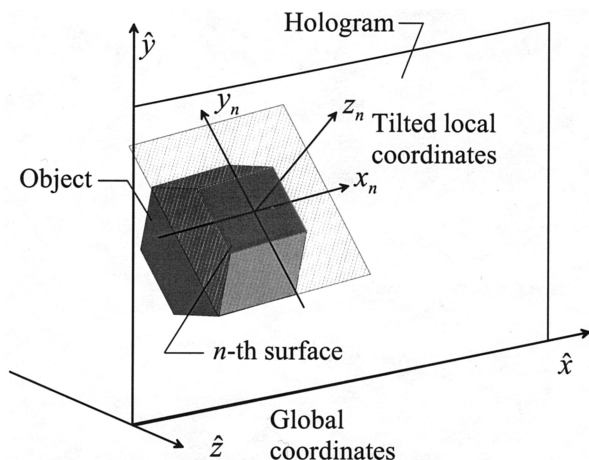
Fig. 1. Geometry and definitions of global coordinates and tilted local coordinates defined for a planar surface.
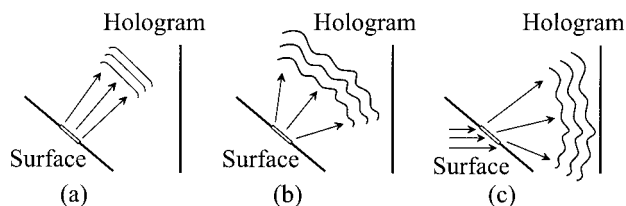

Fig. 2. Fields emitted from surfaces with (a) a constant phase, (b) a diffusive phase, and (c) a diffusive phase multiplied by the phase of a plane wave propagating to a hologram.

of an angular spectrum of plane waves[14] in which remapping the angular spectrum plays an important role. The remapping also eases the difficulty of creating object fields in wave-oriented methods.

In this paper two techniques for synthesizing object fields in surface models are presented for creating 3-D images by use of computer-generated holograms. The first technique, based on the rotational transformation of wave fields presented in Ref. 13 and on remapping of the angular spectrum, provides a method for synthesis of the object fields. This technique makes it possible to create diffusive fields of arbitrarily tilted planar surfaces that have an arbitrary shape and texture. Furthermore, another technique is also presented for avoiding unexpected changes in brightness of the surfaces of objects. The technique enables us to render surface objects as the designers intended.

2. Object Model and the Property Function of Surfaces

The coordinate systems and geometry used in this study are shown in Fig. 1. Objects consist of planar surfaces that are diffusive and luminous by reflecting virtual illumination. Each surface has its own two local coordinates, called tilt and parallel. The tilted local coordinates defined for the nth planar surface are denoted $\mathbf{r}_n = (x_n, y_n, z_n)$, defined such that the planar surface is laid on the $(x_n, y_n, 0)$ plane. A complex function $h_n(x_n, y_n)$ is defined on the plane to give the nth surface such properties as shape, brightness, diffusiveness, and texture. Thus these complex functions are referred to as the property functions of the surface.

Parallel local coordinates $\hat{\mathbf{r}}_n = (\hat{x}_n, \hat{y}_n, \hat{z}_n)$ are also defined for each surface. They share their origin with the tilted coordinates, but the axes are parallel to those of the global coordinates. In the global coordinates, denoted $\mathbf{r} = (\hat{x}, \hat{y}, \hat{z})$, the hologram is placed on the $(\hat{x}, \hat{y}, 0)$ plane. All property functions of surfaces are defined in the following form:

$$h_n(x_n, y_n) = a_n(x_n, y_n)\Psi(x_n, y_n)p_n(x_n, y_n), \quad (1)$$

where $a_n(x_n, y_n)$ is a real function that provides amplitudes of the property function to keep the shape and the texture of the nth surface.

If the property function is defined only as the amplitude distribution, the surface yields little diffusiveness, as shown in Fig. 2(a). For example, $a_n(x_n, y_n)$ in Fig. 1 is a simple rectangular function; i.e., the amplitude is constant within the rectangular surface. This situation is similar to the optical diffraction of a plane wave by a rectangular aperture; therefore, if the surface is visible to the naked eye, the light has not been sufficiently diffracted by the aperture. To give surfaces large diffusiveness, the amplitude functions must be multiplied by a given diffusive phase:

$$\Psi(x_n, y_n) = \exp[ik\phi_d(x_n, y_n)], \quad (2)$$

where $\phi_d(x_n, y_n)$ is a phase that behaves as a numerical diffuser. Random functions are candidates for the diffusive phase, but full random functions are not appropriate to the diffusive phase because the random phases are discontinuous and have a large Fourier frequency. Thus the random phases cause speckles in the reconstruction and problems in numerical calculation. In the research reported in this paper, a digital diffuser proposed for Fourier holograms[15] is used for phase function $\phi_d(x_n, y_n)$.

If a property function is given by the product of the amplitude function and the diffusive phase, the carrier frequency of the field on the tilted $(x_n, y_n, 0)$ plane is zero. This forces the surface to emit light perpendicularly to the surface, as shown in Fig. 2(b). If the surface is sufficiently diffusive, a portion of the emitted field may reach the hologram, but high diffusiveness results in high computational costs such as the need for a great number of sampling points. Therefore the phase of a plane wave propagating perpendicularly to the hologram should be multiplied by the two factors given above. This plane-wave factor causes the field to propagate into the hologram, expressed by

$$p_n(x_n, y_n) = \exp[i(k_{x,n}x_n + k_{y,n}y_n)], \quad (3)$$

where $k_{x,n}$ and $k_{y,n}$ are the x_n and y_n components, respectively, of the wave vector of the plane wave.

The property function given by $h_n(x_n, y_n)$ is transformed into the complex amplitude $\hat{h}_n(\hat{x}_n, \hat{y}_n)$ in the parallel coordinates by the method described in Sec-

tion 5 below. When this transformation is written as

$$\hat{h}_n(\hat{x}_n, \hat{y}_n) = \mathcal{R}_{\theta_x \theta_y \theta_z}\{h_n(x_n, y_n)\}, \qquad (4)$$

fields from all surfaces are superimposed upon the hologram plane as follows:

$$\hat{h}(\hat{x}, \hat{y}) = \sum_n \mathcal{P}_{d_n}\{\hat{h}_n(\hat{x}_n, \hat{y}_n)\}, \qquad (5)$$

where θ_x, θ_y, and θ_z are rotation angles on each axis and $\mathcal{P}_{d_n}\{\}$ represents translational propagation through distance d_n.

3. Rotational Transformation of Property Functions

The details of rotational transformation were already reported in Ref. 13. However, I summarize it for convenience in this section, because rotational transformation of wave fields is the core of techniques proposed in this paper. Note that rotation of just a single planar surface is presented in this section; therefore the subscript n is omitted in this section.

A. Rotation of Coordinates in Fourier Space

The Fourier spectrum of a property function is given in the tilted local coordinates as

$$H(u, v) = \mathcal{F}\{h(x, y)\}$$
$$= \int\!\!\int_{-\infty}^{\infty} h(x, y)\exp[-i2\pi(ux + vy)]\mathrm{d}x\mathrm{d}y, \qquad (6)$$

where u and v denote the Fourier frequencies in the x and y axes, respectively. The frequency in the z axis is not independent of u and v and is given by $w(u, v) = (\lambda^{-2} - u^2 - v^2)^{1/2}$, where λ is the wavelength. The relation among Fourier frequencies in the parallel local coordinates $[\hat{u}, \hat{v}, \hat{w}(\hat{u}, \hat{v})]$ is analogous to this and given by $\hat{w}(\hat{u}, \hat{v}) = (\lambda^{-2} - \hat{u}^2 - \hat{v}^2)^{1/2}$. In Fourier space, the frequencies $[u, v, w(u, v)]$ can be transformed into $[\hat{u}, \hat{v}, \hat{w}(\hat{u}, \hat{v})]$ by ordinary coordinate-transformation procedures and vice versa.

Suppose that $\mathbf{r}$ is transformed into $\hat{\mathbf{r}}$ by a rotation matrix $\mathbf{T}$, i.e., $\hat{\mathbf{r}} = \mathbf{T}\mathbf{r}$ and $\mathbf{r} = \mathbf{T}^{-1}\hat{\mathbf{r}}$. The frequencies in the parallel coordinates are given as

$$u = \alpha(\hat{u}, \hat{v}) = a_1\hat{u} + a_2\hat{v} + a_3\hat{w}(\hat{u}, \hat{v}),$$

$$v = \beta(\hat{u}, \hat{v}) = a_4\hat{u} + a_5\hat{v} + a_6\hat{w}(\hat{u}, \hat{v}), \qquad (7)$$

where the rotation matrix is defined as

$$\mathbf{T}^{-1} = \begin{bmatrix} a_1 & a_2 & a_3 \\ a_4 & a_5 & a_6 \\ a_7 & a_8 & a_9 \end{bmatrix}. \qquad (8)$$

Therefore the spectrum in the parallel coordinates is given by

$$\hat{H}(\hat{u}, \hat{v}) = H[\alpha(\hat{u}, \hat{v}), \ \beta(\hat{u}, \hat{v})]. \qquad (9)$$

Complex amplitudes of the field are obtained in parallel coordinates by inverse Fourier transformation of the spectrum in the paraxial condition[13]:

$$\hat{h}(\hat{x}, \hat{y}) = \mathcal{F}^{-1}\{\hat{H}(\hat{u}, \hat{v})\}$$
$$= \int\!\!\int_{-\infty}^{\infty} \hat{H}(\hat{u}, \hat{v})\exp[i2\pi(\hat{x}\hat{u} + \hat{y}\hat{v})]\mathrm{d}\hat{u}\mathrm{d}\hat{v}. \qquad (10)$$

B. Remapping the Fourier Spectrum

In the actual numerical calculation, to use a FFT one must sample the spectrum as well as the field at an equidistant sampling grid within a given sampling area. The coordinate transformation of Eq. (9), however, causes distortion and a shift of the sampling area and points. This distortion and shift are dependent on the way the tilted local coordinates are defined.[16]

Figure 3(a) shows an example of the definition in which the parallel coordinates $\hat{\mathbf{r}}$ are transformed into the tilted coordinates $\mathbf{r}$ by rotation of the coordinates on the $\hat{z}$ axis before the y axis. In this case, rotation matrix $\mathbf{T}^{-1}$ is given by

$$\mathbf{T}^{-1} = \begin{bmatrix} \cos\theta_y\cos\theta_z & \cos\theta_y\cos\theta_z & -\sin\theta_y \\ -\sin\theta_z & \cos\theta_z & 0 \\ \sin\theta_y\cos\theta_z & \sin\theta_y\sin\theta_z & \cos\theta_y \end{bmatrix}. \qquad (11)$$

Figure 3(b) shows the sampling area of $\hat{H}(\hat{u}, \hat{v})$ for several rotation angles when $h(x, y)$ is sampled at intervals of $\delta_x = \delta_y = 2\ \mu\mathrm{m}$ in $\lambda = 633\ \mathrm{nm}$. The sampling area of $H(u, v)$, a $\delta_x^{-1} \times \delta_y^{-1}$ square, is distorted and shifted. Therefore, resampling accompanied with interpolation is necessary for using an inverse FFT in calculating the complex amplitudes of the field. However, simple interpolation is not sufficient because the FFT algorithm does not work effectively for spectra sampled far from zero frequency. This shift can be interpreted to be a carrier frequency observed in the parallel local coordinates.

Let us reverse the procedure of rotation of the coordinates and shift the origin of Fourier space (u, v) in the tilted coordinates. The origin of Fourier space $(\hat{u}, \hat{v})$ in the parallel coordinates is inversely projected to the frequencies (u_0, v_0) in the tilted coordinates by matrix (8) as follows:

$$u_0 = \alpha(0, 0) = a_3/\lambda, \qquad v_0 = \beta(0, 0) = a_6/\lambda. \qquad (12)$$

To ensure that the center of the spectrum in the parallel coordinates is located at the origin of the Fourier space after rotation of the coordinates, the following new shifted Fourier space should be intro-
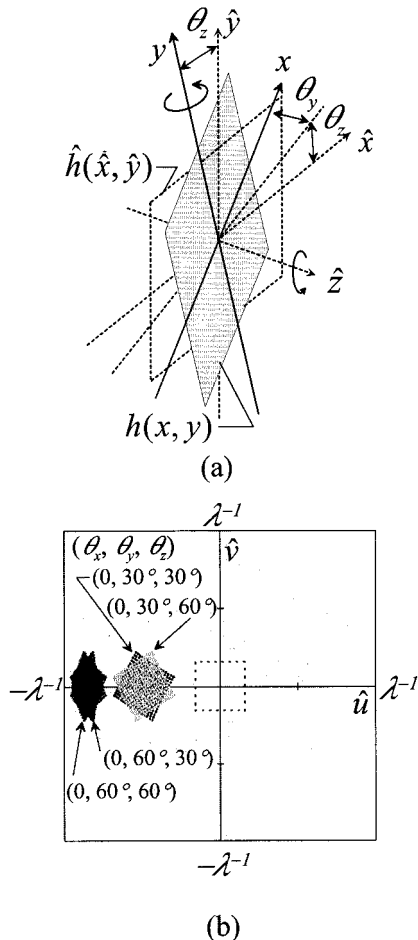
Fig. 3. Schematic of rotation upon two axes: (a) a plane rotated upon the $\hat{z}$ axis before the x axis and (b) resampling areas of the Fourier spectrum at several rotation angles in the rotation scheme.

duced in the tilted coordinates:

$$u' = u - u_0, \qquad v' = v - v_0. \qquad (13)$$

The spectrum expressed in shifted Fourier space (u', v') is written as

$$H'(u', v') = H(u' + u_0, v' + v_0). \qquad (14)$$

The spectrum in the parallel coordinates is obtained by remapping spectrum $H'(u', v')$ onto Fourier space $(\hat{u}, \hat{v})$ as follows:

$$\hat{H}(\hat{u}, \hat{v}) \cong H'(u - u_0, v - v_0)$$
$$= H'(\alpha(\hat{u}, \hat{v}) - u_0, \beta(\hat{u}, \hat{v}) - v_0), \qquad (15)$$

where the sign for nearly equal means that an interpolation is required.

The Fourier spectrum in the shifted Fourier space is obtained by application of the shift theorem of the Fourier-transform theory to Eq. (14):

$$H'(u', v') = \mathscr{F}\{h(x, y)\exp[-i2\pi(u_0x + v_0y)]\}. \quad (16)$$

The exponential factor in brackets in Eq. (16) is attributed to the carrier frequency observed in the parallel coordinates, whereas factor $p(x, y)$ of the property function was introduced to force the emitted field toward the hologram, canceling the carrier frequency in the parallel coordinates. In fact, the exponential factors of Eq. (16) and $p(x, y)$ cancel each other out. Equation (16) is rewritten by substitution of Eq. (3) as follows:

$$H'(u', v') = \mathscr{F}\{a(x, y)\Psi(x, y)\exp\{i[(k_x - 2\pi u_0)x$$
$$+ (k_y - 2\pi v_0)y]\}\}, \qquad (17)$$

where the subscript n is omitted again. The wave vector of a plane wave propagating along the $\hat{z}$ axis is expressed by $(0, 0, 2\pi/\lambda)$ in parallel coordinates. Thus the plane wave in the tilted coordinates is obtained by coordinates rotation by use of matrix (8) as follows:

$$k_x = 2\pi a_3/\lambda, \qquad k_y = 2\pi a_6/\lambda. \qquad (18)$$

The spectrum of relation (15) is rewritten by substitution of Eqs. (18) and (12):

$$H'(u', v') = \mathscr{F}\{a(x, y)\Psi(x, y)\}. \qquad (19)$$

As a result, the factor $p(x, y)$ is no longer required in the property function if the spectrum is calculated in shifted Fourier space (u', v'). Therefore let us redefine the property function as

$$h(x, y) \equiv a(x, y)\Psi(x, y), \qquad (20)$$

and its spectrum as

$$H(u, v) \equiv \mathscr{F}\{h(x, y)\}. \qquad (21)$$

Consequently, the rotational transformation is summarized as follows: First, one obtains spectrum $H(u, v)$ of the property function of Eq. (20) by fast Fourier transformation. The center of the spectrum is placed at the origin in the Fourier space. Next, the spectrum in the parallel coordinates is obtained by remapping spectrum $H(u, v)$, expressed by substituting Eq. (12) into relation (15) as follows:

$$\hat{H}(\hat{u}, \hat{v}) \cong H(\alpha(\hat{u}, \hat{v}) - \alpha(0, 0), \beta(\hat{u}, \hat{v}) - \beta(0, 0)). \qquad (22)$$

Finally, the complex amplitudes of the field are obtained in the parallel coordinates by an inverse Fourier transformation of Eq. (10).

4. Holograms of a Single Surface with Texture

A. Single Axis Rotation

The hologram of a single planar surface with texture was fabricated for verifying the technique described in Section 5. The planar surface and the hologram are
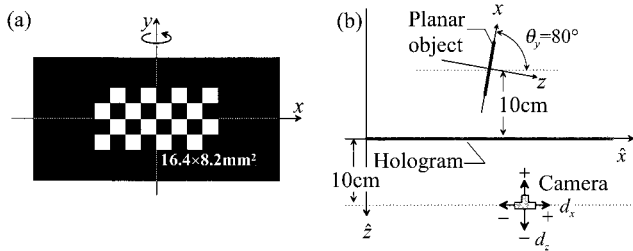
Fig. 4. (a) Planar object used for fabricating the hologram of a plane rotated upon a single axis. (b) Geometry for capturing the reconstruction. The dimensions of texture of a checker embedded in the property function are 16.4 mm × 8.2 mm.

sampled at intervals of 2 μm in the x axis and 4 μm in the y axis. The planar surface has sampling points of 16,384 × 4096 and a binary texture. Amplitude distribution $a(x, y)$ is shown in Fig. 4(a). The surface object was placed at $\hat{z} = -10$ cm and rotated only on the y axis at an angle of 80°, as shown in Fig. 4(b). The hologram with 8192 × 4096 pixels was encoded by a point-oriented method and fabricated by a special printer constructed for printing synthetic fringes.[17]

The hologram is reconstructed by a 633 nm He–Ne laser, and the reconstructed image is captured by a digital camera placed at $\hat{z} = 10$ cm. Figure 5 shows photographs of a reconstructed image. The camera, whose focus is fixed, was moved from left to right for Figs. 5(a)–5(c) and back and forth for Figs. 5(d)–5(f). The apparent size of the texture pattern changes when the viewpoint is moved in Figs. 5(a)–5(c), while the defocused position of the texture pattern changes when the camera is moved because the focal plane of the camera moves in Figs. 5(d)–5(f).

B.   Two-Axis Rotation

Holograms of a single planar surface rotated on two axes were also fabricated and optically reconstructed. The method of rotation of two axes is the same as shown schematically in Fig. 3. The amplitude image with 8192 × 4096 sampling points is shown in Fig. 6.
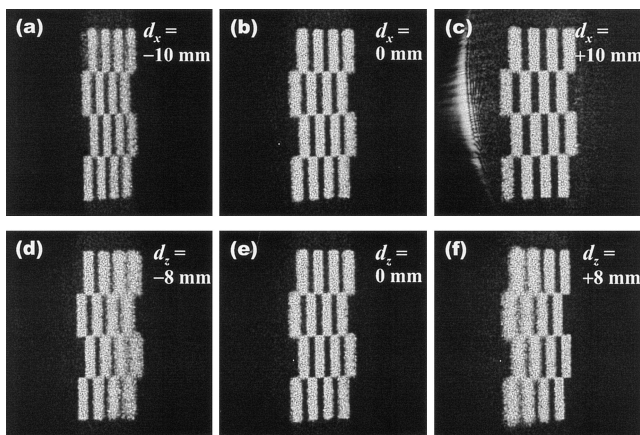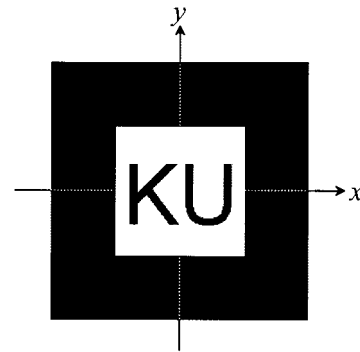

Fig. 6. Planar object used for fabricating a hologram in two-axis rotation.

The number of sampling points and sampling pitches of the hologram is the same as in the single-axis rotation. Optical reconstructions of the holograms are shown in Fig. 7. Four holograms with different rotation angles were fabricated and reconstructed. The appearance of texture on the planar surfaces varies according to the rotation angle.

5.   Holograms of a Three-Dimensional Object and Its Shading

Three-dimensional objects such as cubes and pyramids can be built from planar surfaces. Thus, one can synthesize the fields of these objects by superimposing the fields from the planar surfaces onto the hologram. However, a problem that does not exist when one is synthesizing a single-surface object is that the brightness of the reconstructed surface varies, depending on the angle of the surfaces. As a result, objects are shaded as if an unexpected illumination were throwing light. In a single-surface object, the

Fig. 5. Optically reconstructed images of a hologram captured by moving a camera (a)–(c) from left to right and (d)–(f) back and forth.
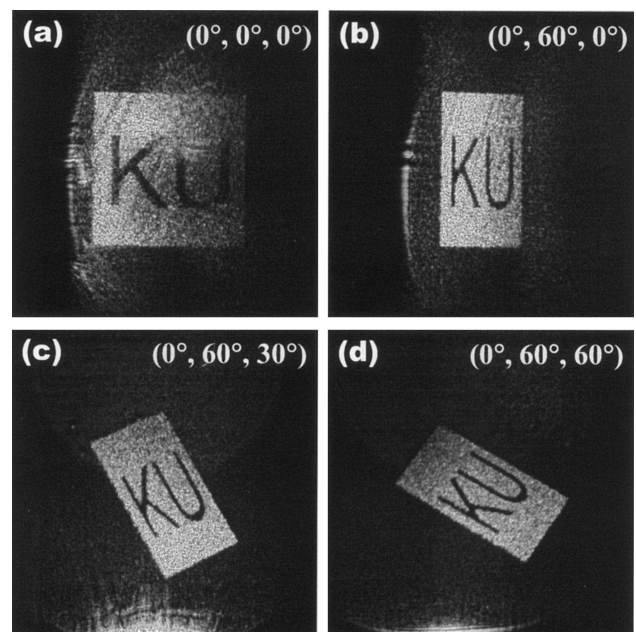

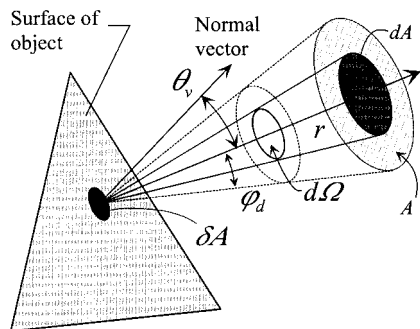Fig. 7. Optical reconstructions of holograms of planar surfaces rotated at several angles.

Fig. 8. Model of brightness of a planar surface expressed by a property function sampled at an equidistant grid.

Fig. 9. Curves of the angle factor for several values of γ.

change of brightness of a surface is not perceived because there is nothing to compare with the single surface in a piece of hologram. This unexpected and unwanted change of brightness must be resolved if one is to shade the object as intended.

A. Theory of Brightness of Reconstructed Surfaces

To compensate for unexpected shading it is necessary to investigate which parameters govern the brightness of the surface in reconstruction. Figure 8 is a theoretical model that predicts the brightness of a surface represented by sampled property function $h(x, y)$. Suppose that the amplitude of a property function of a surface is a constant, i.e., that $a(x, y) \equiv a$, and suppose that a^2 provides optical intensity on the surface. In such cases, the radiant flux Φ of a small area δA on the surface is given by

$$\Phi = \iint_{\delta A} |h(x, y)|^2 \mathrm{d}x\mathrm{d}y$$

$$\cong \delta A \sigma a^2, \tag{23}$$

where σ is the surface density of the sampling points. Assuming that the small area emits light within a diffusion angle in a direction at θ_v to the normal vector, the solid angle corresponding to the diffusion cone is given as $\Omega = A/r^2$, where $A = \pi(r \tan \psi_d)^2$ is the section of the diffusion cone at a distance r and ψ_d is the diffusion angle of light that depends on diffuser function $\Psi(x, y)$ of Eq. (1).

According to photometry, brightness of the surface, observed in a direction at an angle θ_v, is given by

$$L = \frac{\mathrm{d}\Phi/\mathrm{d}\Omega}{\cos \theta_v \delta A}. \tag{24}$$

Assuming that light is diffused almost uniformly, i.e., that $\mathrm{d}\Phi/\mathrm{d}A \simeq \Phi/A$, the brightness is rewritten by substitution of $\mathrm{d}\Phi \simeq (\Phi/A)\mathrm{d}A$, $\mathrm{d}\Omega = \mathrm{d}A/r^2$, and relation (23) into Eq. (24) as follows:

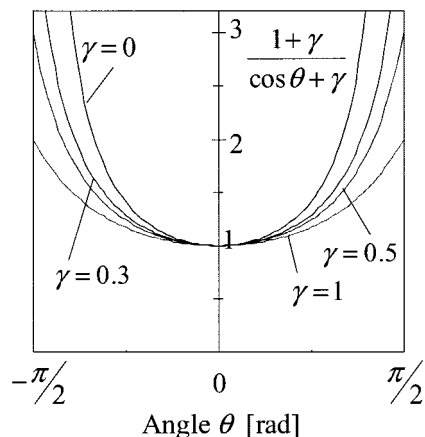$$L \simeq \frac{\sigma a^2}{\pi \tan^2 \psi_d \cos \theta_v}. \tag{25}$$

As a result, the brightness of the surface depends on the surface density of sampling, the diffusiveness of the diffuser function, and the amplitude of the surface property function. In addition, the brightness of the surface is governed by observation angle θ_v. In other words, if several surfaces with the same property function are reconstructed from a hologram, the brightness varies according to the direction of the normal vector of the surface. This phenomenon causes unexpected shading.

Inasmuch as only a simple theoretical model has been discussed so far, relation (25) is only partially appropriate for measuring the brightness of optically reconstructed surfaces of real holograms. The brightness given in relation (25) diverges in the limit $\theta_v \to \pi/2$, but an actual hologram cannot produce infinite brightness for its reconstructed surface. Thus relation (25) is not sufficient to compensate for the brightness. To avoid the divergence of brightness in relation (25), one should introduce angle factor $(1 + \gamma)/(\cos \theta_v + \gamma)$ shown in Fig. 9, instead of $1/\cos \theta_v$, a priori. This angle factor is unity in $\theta_v = 0$ and $1 + 1/\gamma$ in $\theta_v = \pi/2$. Consequently, the brightness is given as an expression of

$$L = \frac{\sigma a^2}{\pi \tan^2 \varphi_d} \frac{(1 + \gamma)}{(\cos \theta_v + \gamma)}, \tag{26}$$

where γ is a parameter that plays a role in preventing the divergence of brightness and in preventing overcompensation. Because γ is dependent on actual methods for fabricating holograms, such as encoding the field or the property of recording materials, it should be determined experimentally.

B. Compensation for Brightness and Shading Objects

The amplitude of a property function that reconstructs a surface in a given brightness L is obtained by solution of Eq. (26) for a as follows:

$$a = \left[\frac{L\pi \tan^2 \varphi_d}{\sigma} \frac{(\cos \theta_v + \gamma)}{(1 + \gamma)} \right]^{1/2}. \tag{27}$$
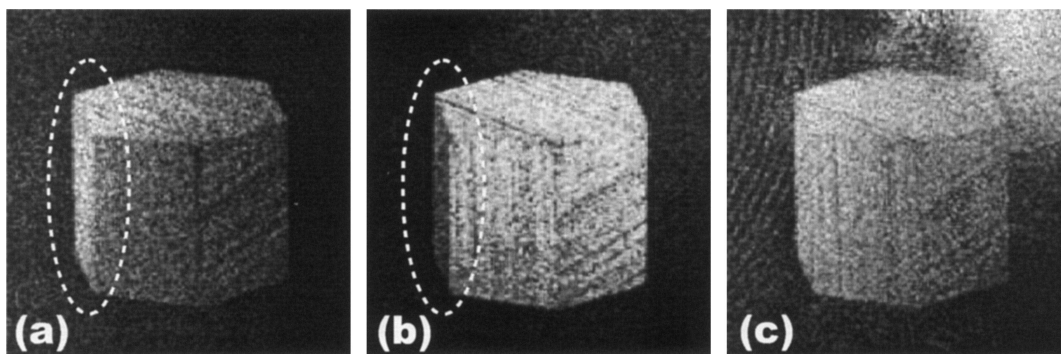
Fig. 10. Optical reconstructions of unshaded hexagonal prisms (a) without brightness compensation and (b), (c) with compensation in $\gamma = 0$, 0.5, respectively.

However, angle θ_v is unknown in synthesizing the object field, and therefore it seems impossible to compensate for the change of brightness. But holograms are observed in a direction along the $\hat{z}$ axis, i.e., perpendicular to the hologram, because the hologram is usually observed at a distance of more than several tens of centimeters. Hence it is possible to approximate θ_v by an angle θ_n formed between the nth surface and the hologram. Objects are shaded by a method based on Lambert's law and the diffused reflection model. The brightness of the nth surface, of which the normal vector forms angle $\hat{\theta}_n$ with the vector of illumination, is given by

$$L_n = L_0(\cos \hat{\theta}_n + l_e), \qquad (28)$$

where l_e is the ratio of the surrounding light to the illumination and L_0 is brightness in $\hat{\theta}_n = 0$ and $l_e = 0$. By substitution of L_n of Eq. (28) into L of Eq. (27) amplitude a_n of the nth surface is given as follows:

$$a_n = a_0 \left[\frac{(\cos \hat{\theta}_n + l_e)(\cos \theta_n + \gamma)}{1 + \gamma} \right]^{1/2}, \qquad (29)$$

$$a_0 \equiv \left[\frac{L_0 \pi \tan^2 \varphi_d}{\sigma} \right]^{1/2}. \qquad (30)$$

Here, observation angle θ_v is replaced by the angle of the normal vector, θ_n.

6. Optical Reconstruction of Three-Dimensional Objects

First, I fabricated several holograms of the same hexagonal prism with which to determine the value of parameter γ. Figure 10 shows the optical reconstruction of three holograms. The reconstructed image of the hologram without compensation for brightness is shown in Fig. 10(a). The left-hand surface of the hexagonal prism, which has the largest angle θ_n, is the brightest of the object surfaces. As shown in Fig. 10(b), the hologram with compensation in $\gamma = 0$ is contrasted to that in Fig. 10(a). Here, remember that compensation in $\gamma = 0$ leads to unlimited compensation. Therefore the surface that forms a large angle with the hologram is dark as a result of overcompensation. Figure 10(c) is also applicable to a hexagonal prism whose brightness is compensated for by $\gamma = 0.5$. Differences of brightness disappear by proper compensation for brightness, which dissolves borders between surfaces.

Figure 11 shows optical reconstruction of 3-D objects whose brightness is completely compensated for at $\gamma = 0.5$. In addition, the surfaces are shaded; the amplitudes of the surfaces are determined by use of Eq. (29) in given virtual illumination and surrounding light. Arrows and numbers in Fig. 11 indicate
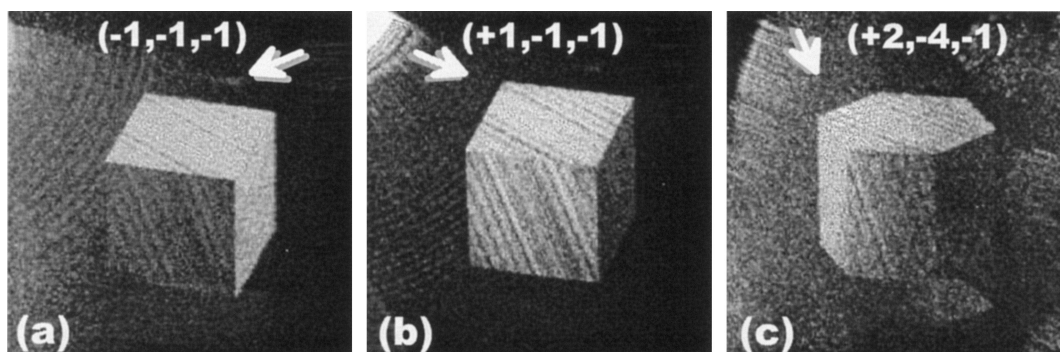

Fig. 11. Optical reconstructions of 3-D objects shaded with illumination light. Cubes are illuminated from the upper right in (a) $l_e = 0$ and from the upper left in (b) $l_e = 0.7$; a hexagonal prism ($l_e = 0.5$) is shown in (c). Brightnesses of objects are all compensated for at $\gamma = 0.5$. Arrows and numbers in parentheses define the illumination vector in global coordinates.

illumination vectors in global coordinates. As expected from the vectors, object surfaces are shaded in the reconstructions.

7. Discussion

The computation time in the proposed techniques is given by rotational transformation of the surfaces of the object. According to Ref. 13, the computation time of rotational transformation is dominated by FFTs, and FFT operation must be executed twice to rotate a planar surface. However, most of the inverse FFTs of Eq. (10) can be omitted from calculating the total field; just an inverse FFT operation is necessary to create a hologram because the translational propagation of the field $\mathcal{P}_d\{\ \}$ can be carried out in Fourier space. In the synthesis of holograms described in previous sections, the method of the angular spectrum of plane waves[14] is used for the operation of the propagation. Therefore the total field of Eq. (5) on the hologram is expressed by

$$\hat{h}(\hat{x}, \hat{y}) = \mathcal{F}^{-1}\Big\{\sum_n \hat{H}_n(\hat{u}_n, \hat{v}_n)\exp[i2\pi\hat{w}(\hat{u}_n, \hat{v}_n)d_n]\Big\}, \tag{31}$$

where d_n is the distance between the $(\hat{x}_n, \hat{y}_n, 0)$ plane of the parallel coordinates and the hologram. Thus the number of times a FFT is executed is $N + 1$, to calculate the total field of an object composed of N pieces of planar surface. As a result, one FFT/surface is approximately estimated as the computational cost in the proposed techniques.

8. Conclusion

Full parallax computer-generated holograms of three-dimensional surface objects were synthesized by use of a wave-optical method. In this method, an object is composed of some planar surfaces, and a complex function defined for each surface retains such properties as shape, texture, and brightness. The fields emitted from the tilted surfaces are calculated by use of the rotational transformation of the property function and totaled on the hologram.

When surfaces build an object, the change of brightness that depends on the angle of view causes unexpected shading of the surface. A theoretical model with which to predict the brightness of the reconstructed surface and prevent unexpected shading has been proposed. This technique allows the object to be shaded as one intends. Finally, optical reconstructions of holograms synthesized by use of the proposed techniques have been demonstrated to verify the validity of the methods.

References

1. J. P. Waters, "Holographic image synthesis utilizing theoretical methods," Appl. Phys. Lett. **9,** 405–407 (1966).
2. A. D. Stein, Z. Wang, and J. J. S. Leigh, "Computer-generated holograms: a simplified ray-tracing approach," Comput. Phys. **6,** 389–392 (1992).
3. M. Lucente, "Interactive computation of holograms using a look-up table," J. Electron. Imag. **2,** 28–34 (1993).
4. J. L. Juárez-Pérez, A. Olivares-Pérez, and R. Berriel-Valdos, "Nonredundant calculation for creating digital Fresnel holograms," Appl. Opt. **36,** 7437–7443 (1997).
5. H. Yoshikawa, S. Iwase, and T. Oneda, "Fast computation of Fresnel holograms employing difference," in *Practical Holography XIV and Holographic Materials VI*, S. A. Benton, S. H. Stevenson, and J. T. Trout, eds., Proc. SPIE **3956,** 48–55 (2000).
6. K. Matsushima and M. Takai, "Recurrence formulas for fast creation of synthetic three-dimensional holograms," Appl. Opt. **39,** 6587–6594 (2000).
7. A. Ritter, J. Böttger, O. Deussen, M. König, and T. Strothotte, "Hardware-based rendering of full-parallax synthetic holograms," Appl. Opt. **38,** 1364–1369 (1999).
8. T. Ito, H. Eldeib, K. Yoshida, S. Takahashi, T. Yabe, and T. Kunugi, "Special purpose computer for holography HORN-2," Comput. Phys. Commun. **93,** 13–20 (1996).
9. D. Leseberg and C. Frère, "Computer-generated holograms of 3-D objects composed of tilted planar segments," Appl. Opt. **27,** 3020–3024 (1988).
10. T. Tommasi and B. Bianco, "Computer-generated holograms of tilted planes by a spatial frequency approach," J. Opt. Soc. Am. A **10,** 299–305 (1993).
11. D. Leseberg, "Computer-generated three-dimensional image holograms," Appl. Opt. **31,** 223–229 (1992).
12. N. Delen and B. Hooker, "Free-space beam propagation between arbitrarily oriented planes based on full diffraction theory: a fast Fourier transform approach," J. Opt. Soc. Am. A **15,** 857–867 (1998).
13. K. Matsushima, H. Schimmel, and F. Wyrowski, "Fast calculation method for optical diffraction on tilted planes by use of the angular spectrum of plane waves," J. Opt. Soc. Am. A **20,** 1755–1762 (2003).
14. J. W. Goodman, *Introduction to Fourier Optics*, 2nd ed. (McGraw-Hill, 1996), Chap. 3.10.
15. R. Bräuer, F. Wyrowski, and O. Bryngdahl, "Diffusers in digital holography," J. Opt. Soc. Am. A **8,** 572–578 (1991).
16. K. Matsushima and A. Kondoh, "Wave optical algorithm for creating digitally synthetic holograms of three-dimensional surface objects," in *Practical Holography XVII and Holographic Materials IX*, T. H. Jeong and S. H. Stevenson, eds., Proc. SPIE **5005,** 190–197 (2003).
17. K. Matsushima and A. Joko, "A high-resolution printer for fabricating computer-generated display holograms (in Japanese)," J. Inst. Image Inf. Television Eng. **56,** 1989–1994 (2002).